UDK 544.65

L.A. Snizhko, N.L. Gurevina, O.A. Kalinichenko, A.A. Chernyshov

ANODIC DEPOSITION OF EXTRINSIC COMPOUNDS

Ukrainian State University of Chemical Engineering

Anodic deposition of own and extrinsic hydroxides on aluminium from electrolyte was studied by voltastatic method at low (0.2−1.0 V) and high (450−600 V) voltages. The mechanism of precipitation was discussed using the conception of fast neutralization coagulation. The models of nucleation-adsorption and nucleation-crystallization mechanism were applied for mathematical simulation of voltastatic curves obtained at low and high voltages correspondingly; appropriate rate constants were calculated.

Introduction

Light metals anodising in diluted alkaline solutions [1, 2] is now of great interest due to development of Plasma Electrolytic Oxidation (PEO) technology. Unfortunately, in spite of great achievements in the technology, the electrochemical nature of the deposition process remains unclear.

The quantitative description of the process that occurs under high voltages includes several stages, as following:

− the part of cathions reaches the outer film surface, enters the electrolyte and gets hydrated;

− in the presence of extrinsic negatively charged anions, for example, inorganic polymers (sodium silicate, tungstate, etc.), the mixture of oxide/hydroxides is accumulated in the adjacent to the electrode layer, lighten the passivity of anode and form insoluble deposits under high temperature [3].

At the same time, both anodic [2] and cathodic [4] deposition of extrinsic compounds occur at the correspondent pH values achieved as a result of water electrolysis accompanied by H^+ (anode) or OH^- (cathode) formation. The nature of deposition can be attributed to the formation of insoluble hydroxides accompanied by charge neutralization coagulation, but the mechanism and kinetics of this process in regards to the PEO technology are yet undefined.

Therefore, the main objective of this paper is developing of electrochemical conception of anodic deposition of extrinsic compounds by analysis of current transients.

Experimental

The preparation of the sample surface and electrolyte compositionis given in [5]. Before low-voltage anodising, the electrode was maintained in the electrolyte until the potential reached (−1.7 V). Each experiment was repeated three times and the average value with the smallest quadratic deviation was used for calculations. The anodising was carried out in a water-cooled glass vessel. A stainless steel counter electrode and a silver/silver chloride reference electrode (0.201 V versus SHE) were used. The anodic polarization was carried out at the constant voltages of 100 to 1500 mV using a potentiostat PI-50 (Russia). The voltages in the range of 450 to 600 V were set by high-voltage power supply linked to a PC. The data were recorded every 80 ms. Numerical simulation of transients was carried out using Mathcad® package.

Results and discussion

Typical current transients for aluminium electrode are shown in the Fig. 1 for two distinct

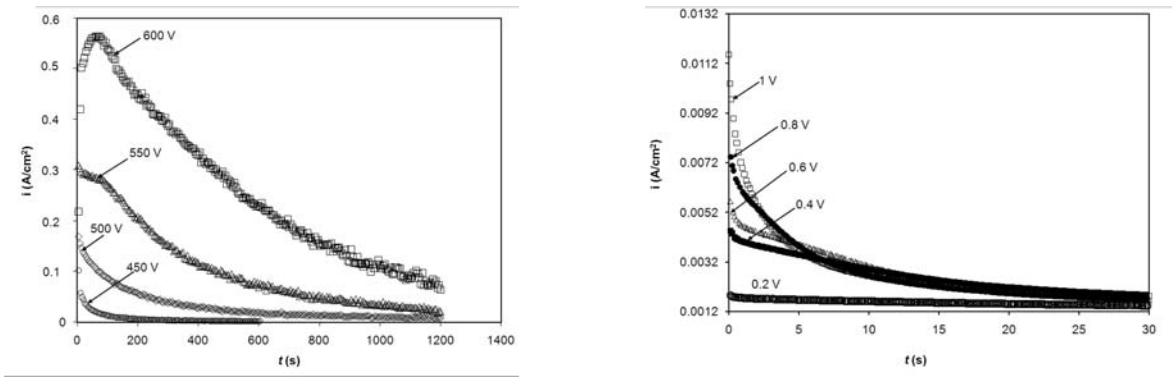

a **b**

Fig. 1. Experimental chronoamperic dependencies obtained under high (a) and low (b) voltages

voltage ranges.

The shape of these transients is similar to that drawn for theoretical transients in the presence of overlap between diffusion fields around growing nuclei [6]. The transients can be divided into three periods. Initially, charging of the double layer leads to a rapid current increase. Then diffusion of Al particles from the underlying metal through the initial oxide film occurs. During the third period, the complicated process of passivation/deposition takes place. Film formation at this stage is limited by growth and increase in the number of nuclei.

Descending parts of voltastatic curves were calculated by the Cottrell equation (1) where all quantities are well known.

$$i(t) = zFC\left(\sqrt{\frac{D}{\pi t}}\right). \quad (1)$$

Full transient curves were described by known equation for 3-dimensional crystal growth [7]:

$$i_{3D} = \frac{k_1}{\sqrt{t}}\theta = \frac{k_1}{\sqrt{t}}\left(1 - e^{-k_2 t^m}\right). \quad (2)$$

Here k_1 and k_2 are the rate constants, θ is the coverage of diffusion zones; t is the time and m reflects the type of crystallization: when m=1 the crystallization is instantaneous, and when m>1 – progressive.

The inclination of $i - \frac{1}{\sqrt{t}}$ dependences (Fig. 2) corresponds to the gently sloping sections of initial i–t curves (passage of the process of dissolution into steady state), which means that the speed of substance supplying is very great at the short times since the effective thickness of diffusion layer is small. Under such conditions, the deceleration of the non-diffusion stages takes place, which are of great interest for kinetic studies.

Simulation results of whole transients according to eq. (2) are shown at the Fig. 3.

It can be seen that the resulting curve is the sum of rising and descending parts. To attain the maximum agreement of calculated and experimental dependences, parameters k_2 and m were adjusted by the least-squares method (Table 1). The value of m=1 seems to be acceptable for the simulation of all types of curves from 450 to 600 voltages. It can be seen, that diffusion coefficients increase with applied potential. Strong dependence between D and

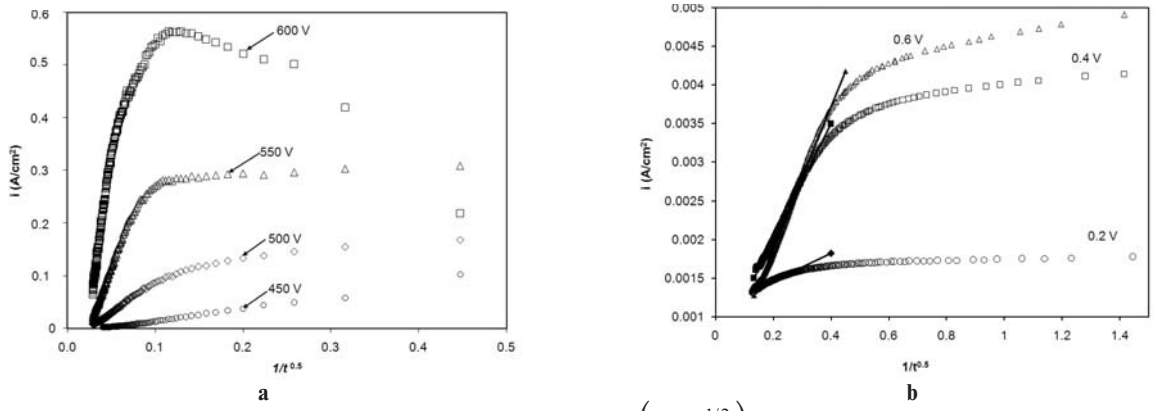

a b

Fig. 2. Treatment of i,t – curves in Cottrels' coordinates $\left(i - t^{-1/2}\right)$ under high (a) and low (b) voltages

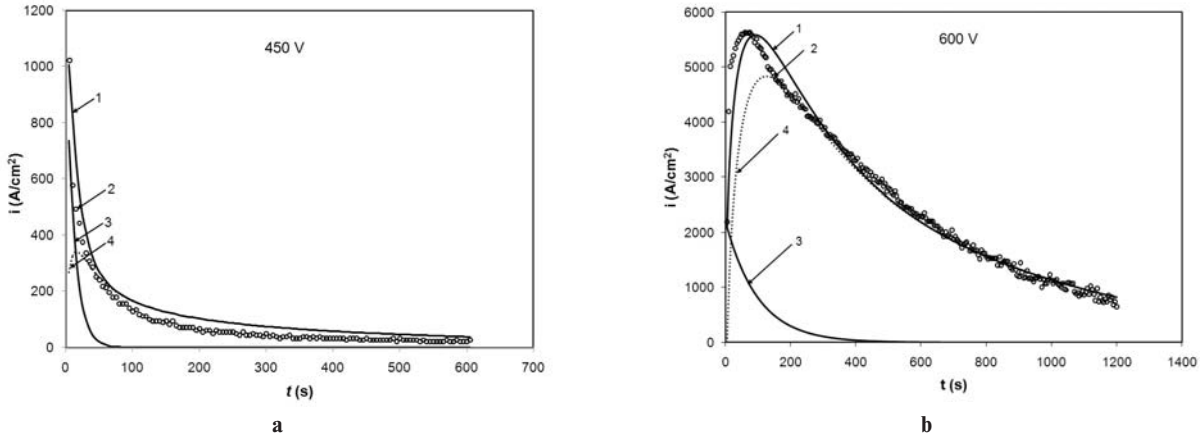

a b

Fig. 3. Typical examples of experimental (1) and calculated (2–4) current transients for potentiostatic anodizing at 450 V (a) and 600 V (b): (2) – total; (3) – partial dissolution; (4) – 3D crystallization

U can be related to the diffusion in a liquid phase.

Table 1

Parameters of equation (1) at the m=1

U, V	i, Am^{-2}	D, cm^2s^{-1}
Low voltages		
0.2	$2.20\cdot10^{-03}$	$5.63\cdot10^{-12}$
0.4	8.110^{-03}	$7.63\cdot10^{-11}$
0.6	$9.33\cdot10^{-03}$	$1.01\cdot10^{-10}$
0.8	$10\cdot10^{-03}$	$1.16\cdot10^{-10}$
1	$12\cdot10^{-03}$	$1.67\cdot10^{-10}$
High voltages		
450	2164	$5.45\cdot10^{-8}$
500	10870	$1.37\cdot10^{-6}$
550	43450	$2.20\cdot10^{-5}$
600	115000	$1.54\cdot10^{-4}$

The constant k_2 as a fitting parameter coincides to the values (0.02−0.04) obtained in the classic work by Phillip et al [7].

Unfortunately, for the low voltages the constant k_2 could not be chosen, which indicates the invalidity of equation (2) for description of deposition process by 3D crystallization mechanism.

For this case, the model for two simultaneous processes such as adsorption and nucleation [8] was applied for low voltages polarisation curves for the best fitting of experimental and calculated data. The basic equation of this model is as follows:

$$i = i_{nucl} + i_{ad} = K_1 t e^{-K_2 t^2} + K_3 e^{-K_4 t}, \quad (3)$$

where K_1, K_2 and K_3, K_4 are the rate constants of nucleation and Langmuir adsorption processes correspondingly;

$$K_1 = 2K_2 q_{nucl}; \quad (4)$$

$$K_3 = K_4 q_{ad}, \quad (5)$$

where q_{nuc1} and q_{ad} − the charges of nucleation and adsorption processes.

Table 2 represents numerical data of constants K_1−K_4 calculated with built-in regression function for experimental i-t dependencies obtained at low potentials.

Table 2

Constants of equation (2)

U, V	K_1	K_2	K_3	K_4
0.2	$1.78\cdot10^{-5}$	$7.26\cdot10^{-4}$	$1.83\cdot10^{-3}$	$2.20\cdot10^{-2}$
0.4	$3.47\cdot10^{-5}$	$1.14\cdot10^{-4}$	$4.89\cdot10^{-3}$	$5.30\cdot10^{-2}$
0.6	$3.52\cdot10^{-5}$	$1.40\cdot10^{-4}$	$6.88\cdot10^{-3}$	$6.80\cdot10^{-2}$
0.8	$7.16\cdot10^{-5}$	$3.57\cdot10^{-4}$	$9.98\cdot10^{-3}$	$1.34\cdot10^{-1}$
1.0	$4.37\cdot10^{-3}$	$8.20\cdot10^{-2}$	$3.21\cdot10^{-3}$	$1.50\cdot10^{-2}$

Fig. 4 shows results of modelling which are typical for chronoamperic dependencies obtained on Al at 0.2−1.0 V.

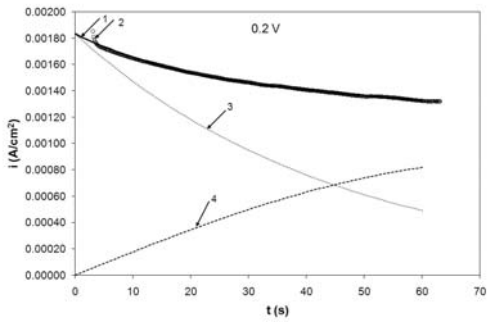

Fig. 4. Mathematical simulation of experimental chronoamperic dependencies according to equation (3) for experimental (1) and calculated (2−4) current transients during low-voltage potentiostatic anodizing. Calculated currents: (2) − total; (3) − adsorption; (4) − nucleation

It can be seen that for all regions a satisfactory correspondence between the experimental and calculated results was observed. It is clear that the adsorption is much faster than nucleation, its' rate reduces slowly and nucleation becomes dominant process with time.

Using values from Table 2 and eq. (4) and (5), it is possible to calculate adsorption and nucleation charges. Relative contribution of each process is presented on Fig. 5. The total charge is distributed almost equally between adsorption and nucleation processes.

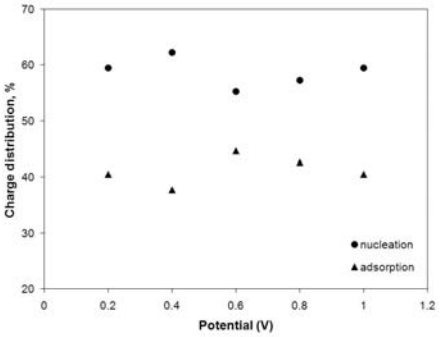

Fig. 5. Percentage ratio between adsorption and nucleation charges at low voltages (<1 V)

The crystalline surface layer with a ratio of aluminium to oxygen of ~3.0 was found overlying the alumina film formed under sparking conditions in the electrolyte of pH 11 at breakdown voltage. It was supposed [2], that it presumably arises from the development of $Al(OH)_3$, either due to hydration of the surface layer or as a byproduct of dielectric breakdown. The layers of insoluble hydroxides were found on the Al surface at the non-sparking anodizing in the solutions of inorganic polymers and the mechanism of deposition formation was explained

by the pH changing in the adjacent to the electrode layer. In the case of aluminium anodising in pure alkaline solutions at high voltages, possible electrochemical and chemical reactions are shownin Table 3. A part of Al cations that reach the film surface enters the electrolyte and gets hydrated. Molecules of insoluble hydroxides are adsorbed on the oxide surface in the form of labile film, which can impede the metal dissolution. In the presence of outside anions derived from electrolyte, the external film surface is covered with mix of oxide/hydroxide compounds, which can both stabilize and dissolve the oxide/hydroxide protective layer (Table 3).

Table 3

Anodic deposition in the adjacent to the electrode layer

Al/oxide film interface	
$Al=Al^{3+}_{solid}+3e^-$	(1)
$2Al^{3+}+3O^{2-}=Al_2O_3$	(2)
Film/electrolyte interface, pH	
$H_2O=0.5O_2+2H^++2e^-$	(3)
$Al(OH)_4^- \xrightarrow{pH=5.6} Al(OH)_3$	(4)
$MnO_4^- \xrightarrow{pH=8.7} Mn(OH)_2$	(5)
$WO_4^{2-} \xrightarrow{pH=2...3} WO_3{\cdot}nH_2O$	(6)
$MoO_4^{2-} \xrightarrow{pH=3} MoO_3{\cdot}nH_2O$	(7)
$SbO_3^- \xrightarrow{pH=6.5} Sb_2O_5{\cdot}nH_2O$	(8)
$SiO_3^{2-} \xrightarrow{pH=6.5} SiO_2{\cdot}nH_2O$	(9)
$VO_3^- \xrightarrow{pH=1.6...6.5} V_2O_5{\cdot}nH_2O$	(10)
Film/electrolyte interface under spark impacts	
$2H_2O-2e^-=H_2O_2+2H^+$	(11
$OH^--e^-=OH^*$	(12)
$OH^*+H_2O_2=H_2O+HO_2^*$	(13)
$OH^*+HO_2^*=H_2O+O_2$	(14)

According to the Faraday's law, we calculated the concentration of generated hydrogen cathions and correspondent pH values in the diffusion layer (150 mm) (Table 4).Initial electrolyte pH was 12.1.

Table 4

pH calculations for voltastatic curves

Low voltages			High voltages		
Voltage (V)	Time (s)	pH	Voltage (V)	Time (s)	pH
0.2	15	11.9–11.3	450	100	10.73–10.56
1.0	15	11.2–10.0	600	100	10.02–9.96
Spark conditions [9]					
Local current density			$20.4{\cdot}10^6$ A/m^2		
Local pH drop in 50 μs spark pulse			7.8		

At the initial pH the Al exists in the solution in a soluble form $Al(H_2O)_6(OH)_4^-$. Due to acidification the amount of insoluble forms increases: in the range of the pH 9...10 solution consists of 60% $Al(H_2O)_3(OH)_3^0$ and 40% $Al(H_2O)_2(OH)_4^-$, at the pH 7.8 the positive (20% $Al(H_2O)_4(OH)_2^+$) and neutral (80% $Al(H_2O)_3(OH)_3$) forms arise.

In regards to the Table 5, the maximum charge of 10^{-3}C of spark burning during 600 ms causes formation of 2.5 mol l^{-1} hydrogen peroxide in 0.001 M NaOH [9].

So, due to the impact of spark discharges, pH of the solution in the near-to the electrode electrolyte layer decreases sharply possibly because of local formation and destruction of hydrogen peroxide.

pH calculations according to the Faraday's low was proven by coincides of calculated and experimental curves obtained by Zhang [10] using a microelectrode technique (Fig. 6).

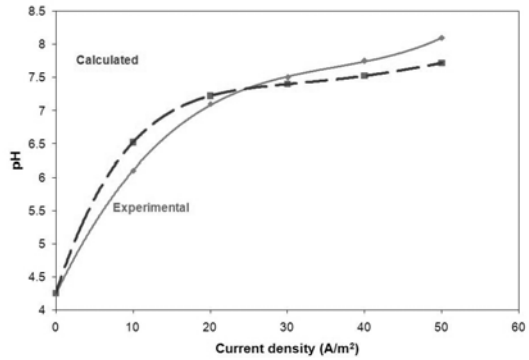

Fig. 6. Experimental and calculated current density – pH dependences

More careful calculations would be obtained taken into account the ionic force of solution g (for example, for 0.05 M KOH γ=0.85) and pH temperature dependence pK_w=0.01706.T+4470.99/T−−6.0875 [11] regarding to the anode heating during electrolysis. Both pH changes and anode heating can cause anodic deposition by sol coagulation when the threshold of coagulation is achieved. For the more accurate theoretical prediction of the possibility of anodic deposition it is necessary to take into account the current density, polarity and temperature in the adjacent to the anode layer.

CONCLUSIONS

1. Current transition curves in a wide range of voltages were analysed in terms of nucleation-diffusion and adsorption-nucleation models and appropriate kinetic constants shows the instantaneous character of deposition.

2. Coagulation of insoluble oxide/hydroxide layer occurs when respective solubility product is

achieved due to sharp decrease/increase of pH value in the adjacent to the electrode layer.

3. Deposition of certain gel substances can be predicted by simple calculations of respective pH as a function of current density and it's polarity.

REFERENCES

1. *Plasma* electrolysis for surface engineering / Yerokhin A., Nie X., Leyland A., Matthews A., Dowey S. // Surface & Coatings Technology. – 1999. – Vol.122. – P.73-93.

2. *Gel* formation and the efficiency of anodic film growth on aluminium / Morlidge J., Skeldon P., Thompson G., Habazaki H., Shimizu K., Wood G. // Electrochim. Acta. – 1999. – Vol.44. – № 14. – P.2423-2435.

3. *Characterisation* of discharge events during plasma electrolytic oxidation / C.S. Dunleavya, I.O. Golosnoyb, J.A. Curran, T.W. Clynea // Surface & Coatings Technology. – 2009. – Vol.203. – № 22. – P.3410-3419.

4. *Eliaz N.*, *Eliyahu M.* Electrochemical processes of nucleation and growth of hydroxyapatite on titanium supported by real-time electrochemical atomic force microscopy // J. of Biomedical Materials Research Part A DOI 10.1002/jbm.a. – 2006. – P.621-634.

5. *Voltastatic* studies of magnesium anodising in alkaline solutions / Snizhko L., Yerokhin A., Gurevina N., Misnyankin D., Ciba A., Matthews A. // Surface & Coatings Technology. – 2010. – Vol.205. – № 5. – P.1527-1531.

6. *Study* on the anodic film formation process of AZ91D magnesium alloy / Zhang L.J., Fan J.J., Zhang Z., Cao F.H., Zhang J.Q., Cao C.N. // Electrochim. Acta. – 2007. – Vol.52. – № 17. – P.5325-5333.

7. *Philipp R.*, *Retter U.* On transition from 2D to 3D nucleation in the anodic film formation of thiourea at the mercury/electrolyte interphase // Electrochim. Acta. – 1995. – Vol.40. – №. 11. – P.1581-1585.

8. *Holzle M.H.*, *Retter U., Kolb D.M.* The kinetics of structural changes in Cu adlayers on Au(111) // J. of Electroanalytical Chemistry. – 1994. – Vol.371. – № 1-2. – P.101-109.

9. *Hickling A. and Ingram M.* Contact glow-discharge electrolysis // Trans. Faraday Soc. – 1964. – Vol.60. – P.783-793.

10. *Mechanistic* studies of electrodeposition for bioceramic coatings of calcium phosphates by an in situ pH-microsensor technique / J.M. Zhang, C.J. Lin, Z.D. Feng, Z.W. Tian // J. of Electroanal. Chemistry. – 1998. – Vol.452. – № 2– P.235-240.

11. *Sven E. Harnung*, *Matthew S.* Johnson Chemistry and the Environment. – Cambridge University Press. – 2012. – 440 p.

Received 5.05.2014